Author Queries

Q1 Kindly check the inserted running title.

Q2 Kindly provide history informations.

Q3 Kindly check the inserted keywords.

Models and finite element techniques for blood flow simulation

M. BEHR†‡*, D. ARORA‡, O. CORONADO‡ and M. PASQUALI‡

†Computational Analysis of Technical Systems, CCES, RWTH Aachen University, Aachen 52056, Germany
‡Chemical and Biomolecular Engineering, Rice University, MS 362, 6100 Main Street, Houston, TX 77005, USA

Recent advances in the area of computational analysis of blood flow devices are presented. Flow simulation techniques relevant to blood pump design based on stabilized finite element formulations and a deforming-mesh space–time approach are outlined, and the results are compared with experimentally-obtained data for a rotary blood pump. Flow prediction is augmented by a strain-based morphology-tensor numerical model capable of quantifying mechanical blood damage. For more accurate representation of blood constitutive behavior, a stabilized finite element formulation for viscoelastic fluids of Oldroyd-B type is also under development. Taken together, this collection of numerical techniques has the potential of significantly improving predictive capabilities of computational fluid dynamics (CFD) during the development stage of blood flow devices.

Keywords: Blood pump design; Ventricular assists devices; Computational fluid dynamics; Red blood cells

1. Introduction

The design of medical devices involving blood flow, such as blood pumps, oxygenators and artificial heart valves, benefits increasingly from computational fluid dynamics (CFD) modeling. In particular, ventricular assists devices (VADs) (Nosé *et al.* 2000) have seen application of numerical techniques (Bludszuweit 1995, Miyazoe *et al.* 1999, Anderson *et al.* 2000, Apel *et al.* 2001, Behr 2004), leading to increased understanding of time-dependent flow fields inside the device, and enabling comparative studies between alternative virtual prototypes. We present our experience in CFD modeling of Baylor GYRO pump (Yoshikawa *et al.* 2000) in Section 2. Beyond CFD analyses of existing devices, firmly in sight is the goal of design optimization, where computer model does not only point out the trends improving the device performance, but also pinpoints the best one in a family of configurations. Yet even the original CFD task of analyzing an existing VAD presents challenges, and unique properties of blood as the circulating fluid need to be addressed.

Blood is a complex fluid—a suspension of red blood cells (RBCs), white blood cells and platelets in a Newtonian liquid (plasma). The first consequence is that blood is susceptible to physiological phenomena not described by fluid mechanics alone. Primary concern here is hemolysis, i.e. premature damage of RBCs, leading to hemolytic anemia. Plasma free hemoglobin released from RBCs is toxic for the kidneys, and can lead to multiple organ failure. Artificial flow devices in particular are capable of producing non-physiological levels of shear stress, which can lead to deformation and fragmentation of RBCs (mechanical hemolysis). The relation between macroscopic flow characteristics, such as shear stress, and microscopic RBC response, such as pore formation or fragmentation, is complicated and not yet fully understood. Available experimental hemolysis data is largely confined to steady shearing flow fields, much different from unsteady flow in VADs. There is also large degree of variability in the hemolytic response depending on the blood species—human, bovine, etc.—and even individual samples. Nevertheless, numerical models for hemolysis are being developed, based principally on the published steady-shear experimental results. In Section 3, we discuss the prevalent stress-based approaches to hemolysis modeling, and the need for a strain-based approach, as exemplified by the morphology-tensor method.

Second consequence of the complex composition of blood is the nonlinear and viscoelastic behavior of this fluid in the macroscale. Although useful qualitative and even quantitative results can be obtained by assuming that blood flow is governed by Navier–Stokes equations of Newtonian fluid, better constitutive models should be used whenever possible. A generalized Newtonian model accounting for the overall shear-thinning behavior is typically the first step, followed by viscoelastic models of rate type, and culminating in multi-scale homogenization-based approaches. In Section 4, we outline the stabilized finite element formulation applicable to flows of complex fluids governed by Oldroyd-B constitutive law.

*Corresponding author. Email: behr@cats.rwth-aachen.de

2   *M. Behr* et al.

We conclude our overview with a summary and point out future research directions in Section 5.

2. Flow modeling

The basis for detailed computational modeling of blood flow are robust and efficient analysis tools providing approximate numerical solutions of the flow governing equations—the incompressible Navier–Stokes equations. Due to complex geometries that needs to be represented, finite difference methods based on overset grids, or more commonly, finite element or volume methods based on unstructured grids, are typically used.

Flow of a viscous incompressible fluid occupying a time-varying n_{sd}-dimensional domain Ω_t with boundary Γ_t is characterized by the velocity $\mathbf{u}(\mathbf{x},t)$ and pressure $p(\mathbf{x},t)$ fields satisfying:

$$\rho(\mathbf{u}_{,t} + \mathbf{u}\cdot\nabla\mathbf{u} - \mathbf{f}) - \nabla\cdot\sigma(\mathbf{u},p) = 0 \ \text{ on } \ \Omega_t, \quad (1)$$

$$\nabla\cdot\mathbf{u} = 0 \ \text{ on } \ \Omega_t, \quad (2)$$

where $\mathbf{f}$ is the body force such as gravity, and the fluid stress is given as:

$$\sigma(\mathbf{u},p) = -p\mathcal{I} + \mathcal{T}(\mathbf{u}), \ \ \mathcal{T}(\mathbf{u}) = 2\mu\mathcal{E}(\mathbf{u}). \quad (3)$$

We denote the symmetric and asymmetric parts of the velocity gradient $\nabla\mathbf{u}$ as $\mathcal{E}(\mathbf{u})$ and $\mathcal{W}(\mathbf{u})$. The fluid density ρ and dynamic viscosity μ are assumed to be constant; alternate constitutive models will be discussed in Section 4. The essential and natural boundary conditions on subsets of the boundary $\Gamma_t = (\Gamma_t)_g \cup (\Gamma_t)_h$ are imposed as $\mathbf{u} = \mathbf{g}$ on $(\Gamma_t)_g$ and $\mathbf{n}\cdot\sigma(\mathbf{u},p) = \boldsymbol{h}$ on $(\Gamma_t)_h$. Together with an initial condition on $\mathbf{u}$, they complete the mathematical statement of the problem.

The unsteady flow problems (1) and (2) is solved using a space–time velocity–pressure stabilized finite element formulation (Behr and Tezduyar 1994): given appropriate velocity and pressure interpolation function spaces for time step $n - (S_{\mathbf{u}}^h)_n$ and $(S_p^h)_n$—as well as corresponding weighting function spaces $(\mathcal{V}_{\mathbf{u}}^h)_n$ and $(\mathcal{V}_p^h)_n$ and given $(\mathbf{u}^h)_n^-$, find $\mathbf{u}^h \in (S_{\mathbf{u}}^h)_n$ and $p^h \in (S_p^h)_n$ such that $\forall \mathbf{w}^h \in (\mathcal{V}_{\mathbf{u}}^h)_n$ and $\forall q^h \in (\mathcal{V}_p^h)_n$:

$$\rho(\mathbf{w}^h, \mathbf{u}_{,t}^h + \mathbf{u}^h\cdot\nabla\mathbf{u}^h - \mathbf{f}^h)_{Q_n} + (\mathcal{E}(\mathbf{w}^h), \sigma(\mathbf{u}^h, p^h))_{Q_n}$$
$$+ (q^h, \nabla\cdot\mathbf{u}^h)_{Q_n} + \sum_{e=1}^{(n_{\text{el}})_n} \frac{\tau}{\rho}\left(\rho\left(\mathbf{w}_{,t}^h + \mathbf{u}^h\cdot\nabla\mathbf{w}^h\right) - \nabla\cdot\sigma(\mathbf{w}^h, q^h),\right.$$
$$\left. \rho\left(\mathbf{u}_{,t}^h + \mathbf{u}^h\cdot\nabla\mathbf{u}^h - \mathbf{f}^h\right) - \nabla\cdot\sigma(\mathbf{u}^h, p^h)\right)_{Q_n^e}$$
$$+ \rho\left((\mathbf{w}^h)_n^+, (\mathbf{u}^h)_n^+ - (\mathbf{u}^h)_n^-\right)_{\Omega^n} = (\mathbf{w}^h, h^h)_{(P_n)_h},$$
$$(4)$$

where $(\mathbf{u}^h)_n^{\pm} = \lim_{\varepsilon\searrow 0}\mathbf{u}(t_n \pm \varepsilon)$ and the domains of integration Q_n, Ω_n, $(P_n)_h$, and the stabilization parameter τ are defined in a standard way (Behr and Tezduyar 1994). More details about this approach, including the shear-slip mesh update method used to account for rotating domain boundaries in the case of rotary blood pumps, as well as, other implementation aspects, can be found in (Behr 2003).

Typical flow simulations using this methodology have been reported in (Behr 2004). They involve the GYRO centrifugal pump under development at the Baylor College of Medicine. The computational domain and a typical finite element mesh is shown in figure 1. Given the finite element model, the hydraulic performance of the device can be readily established. In this type of investigation, the computational problem reproduces experimental conditions, where the pump is run in a test loop mode, using glycerol or blood as test fluid, with varying angular velocity of the impeller. Different levels of clamping are applied to the flow loop tubing, and the resulting flow rate or flux, is recorded and tabulated. In the computations, appropriate pressure head can be applied between Γ_{in} and Γ_{out} corresponding to various clamping levels. At each flow

(a) domain   (b) mesh
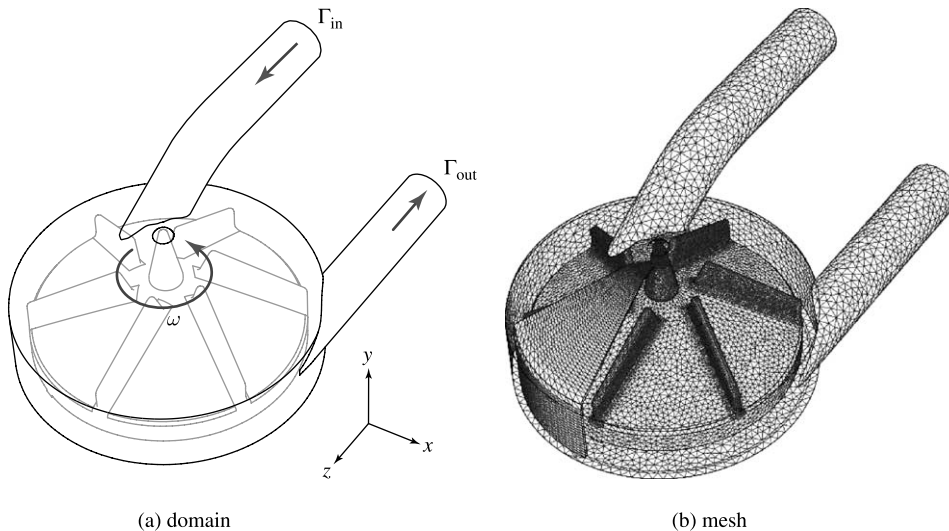
Figure 1.   Computational domain and typical mesh for the GYRO rotary blood pump.
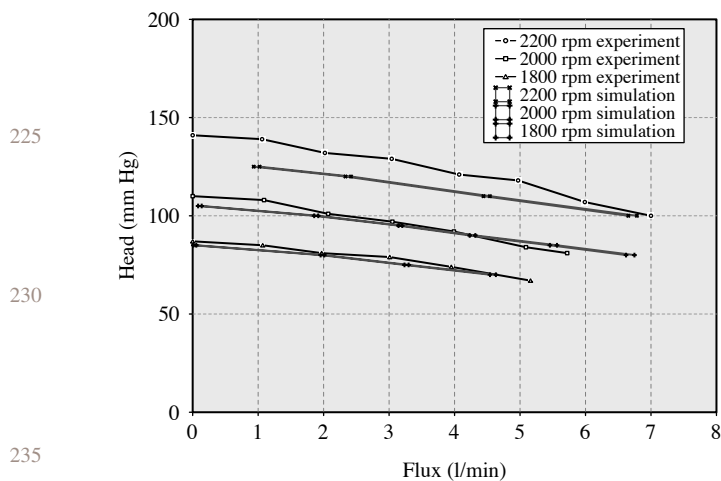
Figure 2. Performance curves for the GYRO rotary blood pump: experiment (black) vs simulation (red).

condition, 4–8 revolutions of the impeller are required for the computed flow field to reach quasi-steady condition.

Three so obtained *performance curves* are plotted in figure 2 for both the experiments and the numerical model, at three angular velocities of 1800, 2000 and 2200 rpm. Multi-valued numerical flux reflects small-scale fluctuations naturally occurring in a time-dependent flow field. The agreement between numerical predictions and experimental values is good at 1800 and 2000 rpm, with larger discrepancy observed at 2200 rpm, possibly due to the limitations of the turbulence model. At lower rpm rates, the numerical analysis is a viable method for predicting pump performance, before the actual prototypes are built. All computations were performed on a Linux PC cluster, with Myrinet interconnect, on partitions ranging from 32 to 72 CPUs, requiring several hours to obtain a quasi-steady flux at each flow condition. Such high computational requirements are balanced by the ease of geometry modification in the numerical model, and by the detailed insight into the flow field.

3. Blood damage modeling

A standard CFD analysis of a blood flow device such as the one discussed in Section 2 can provide important qualitative and quantitative information about the flow field. As in countless other engineering fields, the nature of the flow can be ascertained before any actual prototypes are built, and the design can benefit in its earliest stages from the insights into velocity and pressure distribution obtained via computer modeling. Yet, in contrast to other CFD applications, the topology of the flow field, and even the performance curves shown in figure 2, provide only partial characterization of the device. The raw flow field data do not address the two important aspects of blood flow devices: their hemolytic and thrombogenic properties. Blood damage (hemolysis) and clotting (thrombosis, not discussed here) are of primary importance to long-term successful application of blood pumps. In spite of intense research activity, there is currently no consensus on suitable models that would relate fluid

dynamics information such as stress and shear rate to clinical properties such as normalized index of hemolysis (NIH). In this section, we outline a recently-proposed tensor-based model for blood damage (Arora *et al.* 2004).

A RBC at rest is a biconcave viscoelastic membrane filled with a Newtonian liquid. The membrane has a relaxation time of approximately 200 ms (Hénon *et al.* 1999), and it is capable of supporting an estimated areal strain of 6% before rupturing (Blackshear and Blackshear 1987). The RBCs at rest aggregate into stacked structures called *rouleaux*, which disperse as shear stress increases. The dispersed RBCs preserve their biconcave shape and tumble in a flow with shear stress below ~ 0.1 Pa (Schmid-Schönbein 1969). With increasing shear, the tumbling slows and the cells align with the flow at ~ 0.2 Pa. The RBCs achieve an ellipsoidal shape oriented with the flow at shear stress greater than 1 Pa. An associated tank-treading phenomenon involves the rotation of the outer cell membrane around the enclosed fluid (Williams 1973, Fischer and Stöhr-Liesen 1978). Above 150 Pa, extensive hemolysis occurs due to shear stress alone (Leverett *et al.* 1972), at which point the membrane reaches its areal strain limit.

A correlation for steady-shear hemolysis at short time-scales relevant to flow in blood pumps has been obtained (Giersiepen *et al.* 1990) based on experimental results:

$$\frac{\Delta\text{Hb}}{\text{Hb}} = 3.62 \times 10^{-7} \mathcal{T}^{2.416} \Delta t^{0.785}, \qquad (5)$$

where ($\Delta\text{Hb}/\text{Hb}$) is the ratio of plasma free (released) hemoglobin to the total hemoglobin, $\mathcal{T}$ is the scalar shear stress in Pa, and Δt is exposure time in seconds. From equation (5), the clinically-relevant NIH (American Society for Testing and Materials 1997) can be readily obtained. This correlation was developed for steady-shear hemolysis experiments; however, later studies of blood pumps used in equation (5) a scalar quantity derived from the instantaneous deviatoric stress tensor, e.g. $\mathcal{T} = \sqrt{-(1/2)\mathcal{T} : \mathcal{T}}$. This method of computing hemo-lysis can be called stress-based. A well-known example of this approach is a blood damage model of Bludszuweit (1995), with enhanced models incorporating some aspects of stress threshold and aging, as well as, callibration for a particular device (Yeleswarapu *et al.* 1995, Arvand *et al.* 2004, Goubergrits and Affeld 2004).

An alternative is to approximate the deformation of an RBC in a shear flow by that of a liquid droplet, taking the physical properties of an RBC into consideration. A droplet-deformation equation has been proposed in terms of a symmetric positive-definite morphology tensor that rep-resents the shape of the droplet (Maffettone 1998). The equation takes into consideration the competing action of interfacial tension on droplet surface, which recovers the spherical shape of the droplet, and the force exerted by the surrounding liquid. The equation is frame-invariant and it accounts for non-affine droplet deformation. Although RBCs can be modeled as droplets, the tank-treading motion shown by RBCs is absent in droplets.

The hemolysis model proposed in (Nosé *et al.* 2000) modifies the droplet-deformation equation to account for the tank-treading phenomenon peculiar to RBCs in shear flow, while preserving the frame invariance. In this model, the evolution of the RBC morphology tensor $\mathcal{B}$ is governed by:

$$\frac{d\mathcal{B}}{dt} - [\mathbf{\Omega}\cdot\mathcal{B} - \mathcal{B}\cdot\mathbf{\Omega}] = -f_1[\mathcal{B} - g(\mathcal{B})\mathcal{I}]$$
$$+ f_2[\widetilde{\mathcal{E}}\cdot\mathcal{B} + \mathcal{B}\cdot\widetilde{\mathcal{E}}]$$
$$+ f_3[\widetilde{\mathcal{W}}\cdot\mathcal{B} - \mathcal{B}\cdot\widetilde{\mathcal{W}}], \quad (6)$$

where $g(\mathcal{B}) = (3III/II)$ (involving third and second invariant of $\mathcal{B}$), $f_1 = 5.0\,\text{s}^{-1}$ based on RBC relaxation time, and $f_2 = f_3 = 1.25 \times 10^{-3}$ are uniquely determined by RBC behavior in steady shear flow (Nosé *et al.* 2000). The orthonormal matrix $\mathbf{\Omega}$ defines the rate of rotation of a reference frame attached to the eigenvectors of $\mathcal{B}$, leading to $\widetilde{\mathcal{E}} = \mathcal{E}$, and $\widetilde{\mathcal{W}} = \mathcal{W} - \mathbf{\Omega}$.

The morphology tensor evolution is tracked with equation (6) along pathlines, providing information about the deformation, or strain, of the RBC at each point in the flow field. An instantaneous deformation of the RBC can be uniquely associated with a hypothetical steady shear flow that would generate such a deformation, and thus, matched with a hemolysis rate using experimental correlation (5) (Nosé *et al.* 2000). That rate can be in turn integrated along each pathline, and information from many pathlines averaged, to provide hemolysis release information for the entire device. To distinguish from models using instantaneous stress values which assume immediate response of the RBC to the surrounding flow field, the model based on the morphology tensor $\mathcal{B}$ is referred to as strain-based. The difference between strain- and stress-based approaches to hemolysis modeling is schematically shown in figure 3.

Comparison of this strain-based model with standard stress-based approach showed significant over-estimation of hemolysis when using the latter in the context of a test two-dimensional (2D) pump geometry (Nosé *et al.* 2000). Initial three-dimensional (3D) results also indicate that the strain-based model leads to lower predicted values of NIH, which are more in line with the experimental results. A typical set of streamlines in the GYRO device at 2000 rpm and $51\,\text{min}^{-1}$ flow rate is shown in figure 4, with each streamline colored by cumulative hemolysis release (ΔHb/Hb). The resulting NIH values, predicted using the stress- and a strain-based model are compared to the experimentally-obtained value (Yuri *et al.* 2004) in table 1. Although the close agreement between experiment and strain-based hemolysis prediction awaits further testing and may be a coincidence, it is clearly seen that the stress-based model overestimates the hemolysis by a factor of three.

4. Viscoelastic modeling

Blood flow in artificial devices is typically modeled using a Newtonian constitutive model described in Section 2. A more accurate description of the constitutive behavior of the blood as a fluid is a generalized Newtonian model—in particular, the Carreau-Yasuda model (Gijsen *et al.* 1999, Leuprecht, 2001). Although easy to implement, a generalized Newtonian model leads to additional non-linearities in the equation system and complicates the task of achieving convergence at each time step of the simulation. In our experience, an application of the shear-thinning model gives largely the same global behavior, e.g. the performance curves from figure 2, as those obtained when using a Newtonian simplification. For other tasks, such as shape optimization,
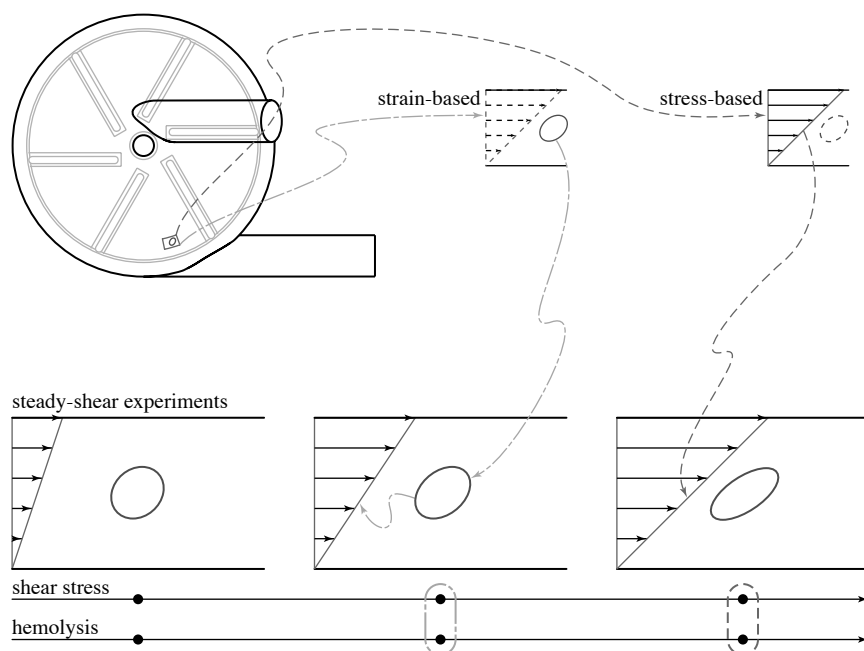
Figure 3.   Strain- and stress-based approaches to hemolysis modeling: RBC deformation (red) matched with an equivalent steady stress vs assumed instantaneous response of the RBC to a given fluid stress.
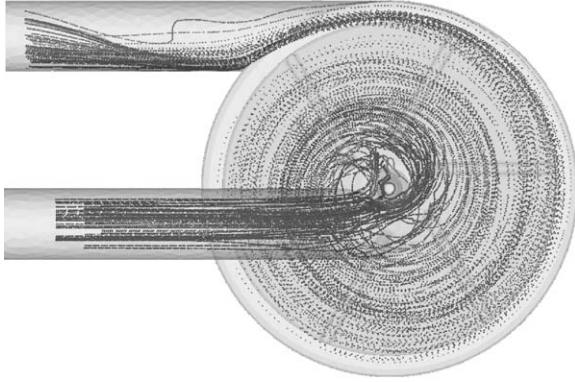
Figure 4. Flow in a GYRO blood pump: pathlines used for NIH computation color-coded by accumulated hemoglobin release.

significant differences in the outcome has been observed depending on the constitutive model (Abraham *et al.* 2004). Since an even more accurate description of blood constitutive behavior has been identified as a modified Oldroyd-B model (viscoelastic fluid in a shear-thinning solvent) (Yeleswarapu 1996), we are also interested in developing robust and efficient finite element techniques for this type of complex fluids. Viscoelastic fluids of rate type present a number of numerical challenges: the advective nature of the constitutive equations, and the interaction of multiple discrete unknown fields—viscoelastic stress, velocity and pressure. Adding the streamline-upwind/petrov-galerkin (SUPG) terms (Marchal and Crochet 1987) to the Galerkin formulation, or using the discontinuous-galerkin (DG) approach (Fortin 1989), was instrumental in overcoming the difficulties associated with the advective terms in the constitutive equation. Compatibility conditions on stress and velocity interpolations were identified (Fortin and Pierre 1987) and first satisfied by complex combinations of interpolation functions. Later methods allowed simpler equal-order interpolations for the viscoelastic stress and velocity, such as the discrete elastic viscous stress splitting (DEVSS) approaches—DEVSS-G/SUPG (Guénette and Fortin 1995, Szady *et al.* 1995) and DEVSS-G/DG (Sun *et al.* 1999).

For an Oldroyd-B fluid, the governing equations (1) and (2) are supplemented by a constitutive equation:

$$\boldsymbol{\sigma} = -p\mathcal{I} + \boldsymbol{\mathcal{T}}_1 + \boldsymbol{\mathcal{T}}_2, \quad \boldsymbol{\mathcal{T}}_1 + \lambda\overset{\triangledown}{\boldsymbol{\mathcal{T}}}_1 = 2\mu_1\mathcal{E}(\mathbf{u}),$$
$$\boldsymbol{\mathcal{T}}_2 = 2\mu_2\mathcal{E}(\mathbf{u}), \qquad (7)$$

where the $\overset{\triangledown}{\boldsymbol{\mathcal{T}}}$ denotes an upper-convected derivative:

$$\overset{\triangledown}{\boldsymbol{\mathcal{T}}} = \boldsymbol{\mathcal{T}}_{,t} + \mathbf{u}\cdot\boldsymbol{\nabla}\boldsymbol{\mathcal{T}} - (\boldsymbol{\nabla}\mathbf{u}\boldsymbol{\mathcal{T}} + \boldsymbol{\mathcal{T}}(\boldsymbol{\nabla}\mathbf{u})^T), \qquad (8)$$

Table I. Hemolysis in a GYRO blood pump: NIH values for numerical models and the experiment.

	Hemolysis [g/100l]
Stress-based model	0.0200
Strain-based model	0.0069
Experiment	0.0073

and μ_1 and μ_2 are the viscoelastic and solvent viscosities, respectively.

Substituting $\boldsymbol{\mathcal{T}}_2$ directly into equation (1) and dropping the subscript from $\boldsymbol{\mathcal{T}}_1$, the GLS3 velocity–pressure–stress formulation for Oldroyd-B fluid is written as follows: given $(\mathbf{u}^h)_n^-$ and $(\boldsymbol{\mathcal{T}}^h)_n^-$, find $\mathbf{u}^h \in (S_{\mathbf{u}}^h)_n$, $p^h \in (S_p^h)_n$ and $\boldsymbol{\mathcal{T}}^h \in (\mathcal{S}_{\mathcal{T}}^h)_n$ such that $\forall \mathbf{w}^h \in (\mathcal{V}_{\mathbf{u}}^h)_n$, $\forall q^h \in (\mathcal{V}_p^h)_n$ and $\forall \mathcal{S}^h \in (\mathcal{V}_{\mathcal{T}}^h)_n$:

$$\rho\Big(\mathbf{w}^h, \mathbf{u}_{,t}^h + \mathbf{u}^h\cdot\nabla\mathbf{u}^h - \mathbf{f}\Big)_{Q_n} - \big(\nabla\cdot\mathbf{w}^h, p^h\big)_{Q_n}$$

$$+ \big(\mathcal{E}(\mathbf{w}^h), \boldsymbol{\mathcal{T}}^h + 2\mu_2\mathcal{E}(\mathbf{u}^h)\big)_{Q_n} + \big(q^h, \nabla\cdot\mathbf{u}^h\big)_{Q_n}$$

$$+ \Big(\mathcal{S}^h, \frac{1}{2\mu_1}\boldsymbol{\mathcal{T}}^h + \frac{\lambda}{2\mu_1}\overset{\triangledown}{\boldsymbol{\mathcal{T}}}^h - \mathcal{E}(\mathbf{u}^h)\Big)_{Q_n}$$

$$+ \sum_{e=1}^{n_{\text{el}}} \frac{\tau_{\text{MOM}}}{\rho}\Big(\rho\big(\mathbf{w}_{,t}^h + \mathbf{u}^h\cdot\nabla\mathbf{w}^h + \nabla q^h - \nabla\cdot\mathcal{S}^h\big)$$

$$- 2\mu_2\nabla\cdot\mathcal{E}(\mathbf{w}^h), \rho\Big(\mathbf{u}_{,t}^h + \mathbf{u}^h\cdot\nabla\mathbf{u}^h - \mathbf{f}\Big) \qquad (9)$$

$$+ \nabla p^h - \nabla\cdot\boldsymbol{\mathcal{T}}^h - 2\mu_2\nabla\cdot\mathcal{E}(\mathbf{u}^h)\big)_{Q_n^e} + \sum_{e=1}^{n_{\text{el}}} 2\mu_1\tau_{\text{CONS}}$$

$$\times \Big(\frac{1}{2\mu_1}\mathcal{S}^h + \frac{\lambda}{2\mu_1}\overset{\triangledown}{\mathcal{S}}^h - \mathcal{E}(\mathbf{w}^h), \frac{1}{2\mu_1}\boldsymbol{\mathcal{T}}^h + \frac{\lambda}{2\mu_1}\overset{\triangledown}{\boldsymbol{\mathcal{T}}}^h - \mathcal{E}(\mathbf{u}^h)\Big)_{Q_n^e}$$

$$+ \rho\Big((\mathbf{w}^h)_n^+, (\mathbf{u}^h)_n^+ - (\mathbf{u}^h)_n^-\Big)_{\Omega_n}$$

$$+ \frac{\lambda}{2\mu_1}\Big((\mathcal{S}^h)_n^+, (\boldsymbol{\mathcal{T}}^h)_n^+ - (\boldsymbol{\mathcal{T}}^h)_n^-\Big)_{\Omega_n} = (\mathbf{w}^h, \mathbf{h}^h)_{(P_n)_h},$$

where $(S_{\mathbf{u}}^h)_n$ and $(\mathcal{V}_{\mathbf{u}}^h)_n$ are the space–time extensions of appropriately defined interpolation and weighting function spaces for velocity, pressure and the deviatoric viscoelastic stress (Miyazoe *et al.* 1999).

As in equation (4), standard stabilization parameter τ_{MOM} is used. The parameter τ_{CONS} is:

$$\tau_{\text{CONS}} = \left(1 + \left(\frac{2\lambda|\mathbf{u}^h|}{h}\right)^2 \big(\lambda|\nabla\mathbf{u}^h|\big)^2\right)^{\frac{1}{2}}, \qquad (10)$$

resulting in better behavior at low Weissenberg numbers than the one used in (Behr *et al.* 2004). Two variations of GLS3 formulation were introduced in (Behr *et al.* 2004), which involve decoupled recovery of continuous velocity gradient using consistent (GLS3-M) and lumped (GLS3-L) mass matrix. These improve consistency of the stabilization terms in the presence of Newtonian solvent.

A subset of this formulation suitable for steady flows has been recently applied to the benchmark problem, involving flow of an Oldroyd-B fluid past a circular cylinder placed between parallel fixed plates, with channel width being eight times the cylinder diameter (Behr *et al.* 2004). One of the characteristic flow quantities is the drag

6   *M. Behr* et al.
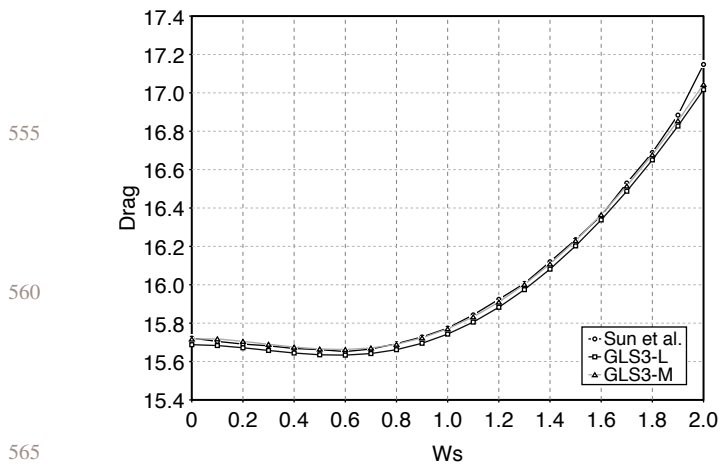
Figure 5.   Viscoelastic flow past a circular cylinder: drag as a function of Weissenberg number.

on the cylinder as a function of the Weissenberg number, shown in figure 5. The agreement between GLS3-M, GLS3-L and DEVSS-G/SUPG results of Sun *et al.* (1999) is excellent up to Weissenberg number of 1.8.

5. Concluding remarks

We have presented an overview of our recent efforts in the area of computational analysis of blood flow devices. We have described an application of flow simulation techniques relevant to blood pump design. Our approach is based on stabilized finite element formulations, and a deforming-mesh space–time approach, with the shear-slip mesh update technique used to accommodate a rotating impeller. Owing to portable parallel implementation, our time-accurate simulations are performed on parallel clusters of commodity computers. The agreement with experimentally-observed flow characteristics is satisfactory, save for high impeller rotation rates which are believed to expose shortcomings in turbulence modeling. For clinical relevance, the CFD analysis needs to be accompanied by hemolysis prediction, and to this end, we have introduced a tensor-deformation model that mimics roughly the behavior of red blood cells in the flow field. The Lagrangian approach used currently should be re-derived in an Eulerian form for increased cost-effectiveness. For added accuracy, we are also developing robust and efficient ways of accounting for complex constitutive behavior of blood and in particular, a stabilized finite element formulation for viscoelastic fluids of Oldroyd-B type. Testing of this new formulation is still focused on 2D benchmarks, with 3D benchmarks and applications still to follow.

Acknowledgements

References

Abraham, F., Behr, M. and Heinkenschloss, M., Shape optimization in stationary blood flow: a numerical study of non-Newtonian effects. submitted to *Comput. Methods Biomech. Biomed. Eng.*, 2004.

American Society for Testing and Materials, Standard practice for assessment of hemolysis in continuous flow blood pumps, Standard F 1841–97, ASTM, 1997.

Anderson, J.B., Wood, H.G., Allaire, P.E., Bearnson, G. and Khanwilkar, P., Computational flow study of the continuous flow ventricular assist device, prototype number 3 blood pump. *Artif. Org.*, 2000, **24**, 377–385.

Apel, J., Paul, R., Klaus, S., Siess, T. and Reul, H., Assessment of hemolysis related quantities in a microaxial blood pump by computational fluid dynamics. *Artif. Org.*, 2001, **25**, 341–347.

Arora, D., Behr, M. and Pasquali, M., A tensor-based measure for estimating blood damage. *Artif. Org.*, 2004, **28**, 1002–1015.

Arvand, A., Hahn, N., Hormes, M., Akdis, M., Martin, M. and Reul, H., Comparison of hydraulic and hemolytic properties of different impeller designs of an implantable rotary blood pump by computational fluid dynamics. *Artif. Org.*, 2004, **28**, 892–898.

Behr, M., On the application of slip boundary condition on curved boundaries. *Int. J. Num. Methods Fluids*, 2004, **45**, 43–51.

Behr, M. and Tezduyar, T.E., Finite element solution strategies for large-scale flow simulations. *Comput. Methods Appl. Mech. Eng.*, 1994, **112**, 3–24.

Behr, M. and Arora, D., Shear-slip mesh update method: implementation and applications. *Comput. Methods Biomech. Biomed. Eng.*, 2003, **6**, 113–123.

Behr, M., Arora, D., Coronado-Matutti, O. and Pasquali, M., Stabilized finite element methods of GLS type for Oldroyd-B viscoelastic fluid. In *Proceedings of the European Congress on Computational Methods in Applied Science and Engineering ECCOMAS 2004*, edited by P. Neittaanmäki, T. Rossi, J. O nate, J. Périaux and D. Knörzer, 2004 (ECCOMAS: Jyväskylä, Finland).

Blackshear, P.L. and Blackshear, G.L., Mechanical hemolysis. In *Handbook of Bioengineering*, edited by R. Skalak and S. Chien, pp. 15.1–15.19, 1987 (McGraw-Hill: New York).

Bludszuweit, C., Three-dimensional numerical prediction of stress loading of blood particles in a centrifugal pump. *Artif. Org.*, 1995, **19**, 590–596.

Fischer, T.M., Stöhr-Liesen, M. and Schmid-Schönbein, H., The red cell as a fluid droplet: Tank tread-like motion of the human erythrocyte membrane in shear flow. *Science*, 1978, **202**, 894–896.

Fortin, M. and Fortin, A., A new approach for the FEM simulation of viscoelastic flows. *J. Non-Newtonian Fluid Mech.*, 1989, **32**, 295–310.

Fortin, M. and Pierre, R., On the convergence of the mixed method of Crochet and Marchal for viscoelastic flows. *Comput. Methods Appl. Mech. Eng.*, 1987, **7**, 1035–1052.

Giersiepen, M., Wurzinger, L.J., Opitz, R. and Reul, H., Estimation of shear stress-related blood damage in heart valve prostheses—*in vitro* comparison of 25 aortic valves. *Int. J. Artif. Org.*, 1990, **13**, 300–306.

Gijsen, F.J.H., van de Vosse, F.N. and Janssen, J.D., The influence of the non-newtonian properties of blood on the flow in large arteries: steady flow in a carotid bifurcation model. *J. Biomech.*, 1999, **32**, 601–608.

Goubergrits, L. and Affeld, K., Numerical estimation of blood damage in artificial organs. *Artif. Org.*, 2004, **28**, 499–507.

Guénette, R. and Fortin, M., A new mixed finite element method for computing viscoelastic flows. *J. Non-Newtonian Fluid Mech.*, 1995, **60**, 27–52.

Hénon, S., Lenormand, G., Richert, A. and Gallet, F., A new determination of the shear modulus of the human erythrocyte membrane using optical tweezers. *Biophysical J.*, 1999, **76**, 1145–1151.

Leuprecht, A. and Perktold, K., Computer simulation of non-newtonian effects on blood flow in large arteries. *Comput Methods Biomech Biomed Eng*, 2001, **4**, 149–163.

Leverett, L.B., Hellums, J.D., Alfrey, C.P. and Lynch, E.C., Red blood cell damage by shear stress. *Biophysical J.*, 1972, **12**, 257–273.

Maffettone, P.L. and Minale, M., Equation of change for ellipsoidal drops in viscous flow. *J. Non-Newtonian Fluid Mech.*, 1998, **78**, 227–241.

Marchal, J.M. and Crochet, M.J., A new mixed finite element for calculating viscoelastic flow. *J. Non-Newtonian Fluid Mech.*, 1987, **26**, 77–114.

Miyazoe, Y., Sawairi, T., Ito, K., Konishi, Y., Yamane, T., Nishida, M., Asztalos, B., Masuzawa, T., Tsukiya, T., Endo, S. and Taenaka, Y., Computational fluid dynamics analysis to establish the design process of a centrifugal blood pump: second report. *Artif. Org.*, 1999, **23**, 762–768.

Nosé, Y., Yoshikawa, M., Murabayashi, S. and Takano, T., Development of rotary blood pump technology: past, present, and future. *Artif. Org.*, 2000, **24**, 412–420.

Schmid-Schönbein, H. and Wells, R., Fluid drop-like transition of erythrocytes under shear. *Science*, 1969, **165**, 288–291.

Sun, J., Smith, M.D., Armstrong, R.C. and Brown, A., Finite element method for viscoelastic flows based on the discrete adaptive viscoelastic stress splitting and the discontinuous Galerkin method: DAVSS-G/DG. *J. Non-Newtonian Fluid Mech.*, 1999, **86**, 281–307.

Szady, M.J., Salamon, T.R., Liu, A.W., Armstrong, R.C. and Brown, A., A new mixed finite element method for viscoelastic flows governed by differential constitutive equations. *J. Non-Newtonian Fluid Mech.*, 1995, **59**, 215–243.

Williams, A.R., Shear-induced fragmentation of human erythrocytes. *Biorheology*, 1973, **10**, 303–311.

Yeleswarapu, K.K., Antaki, J.F., Kameneva, M.V. and Rajagopal, R., A mathematical model for shear-induced hemolysis. *Artif. Org.*, 1995, **19**, 576–582.

Yeleswarapu, K.K., Evaluation of continuum models for characterizing the constitutive behavior of blood. Ph.D. thesis, University of Pittsburgh, Department of Mechanical Engineering, 1996.

Yoshikawa, M., Nonaka, K., Linneweber, J., Kawahito, S., Ohtsuka, G., Nakata, K., Takano, T., Schulte-Eistrup, S., Glueck, J., Schima, H., Wolner, E. and Nosé, Y., Development of the NEDO implantable ventricular assist device with gyro centrifugal pump. *Artif. Org.*, 2000, **24**, 459–467.

Yuri, K., Iwahashi, H., Motomura, T., Hata, A., Asai, T., Nosé, Y., Arora, D., Behr, M. and Pasquali, M., Different levels of hemolysis occurred by a centrifugal blood pumps in various clinical conditions. *ASAIO J.*, 2004, **50**, ASAIO 50th Anniversary Conference Abstracts 121.